Color switching of a terahertz quantum cascade laser

Martin A. Kainz 🆔 , Sebastian Schönhuber, Benedikt Limbacher, Aaron M. Andrews 🆔 , Hermann Detz 🆔 ,
Gottfried Strasser 🆔 , Gérald Bastard, and Karl Unterrainer 🆔

View Online   Export Citation   CrossMark

ARTICLES YOU MAY BE INTERESTED IN

Color switching of a terahertz quantum cascade laser

Martin A. Kainz,[1,2,a] Sebastian Schönhuber,[1,2] Benedikt Limbacher,[1,2] Aaron M. Andrews,[2,3]
Hermann Detz,[2,4] Gottfried Strasser,[2,3] Gérald Bastard,[1,5] and Karl Unterrainer[1,2]

AFFILIATIONS

[1]Photonics Institute, TU Wien, 1040 Vienna, Austria
[2]Center for Micro- and Nanostructures, TU Wien, 1040 Vienna, Austria
[3]Institute of Solid State Electronics, TU Wien, 1040 Vienna, Austria
[4]Central European Institute of Technology, Brno University of Technology, 61200 Brno, Czech Republic
[5]Laboratoire de Physique de l'Ecole Normale Supérieure, PSL Research University, 75005 Paris, France

[a]Electronic mail: martin.kainz@tuwien.ac.at

ABSTRACT

The mode formation of a terahertz Quantum Cascade laser with two optical transitions is studied experimentally. The emission spectrum shows two well separated frequency regions at 3.4 THz and 3.8 THz corresponding to two different upper laser states $|3\rangle$ and $|4\rangle$. From the relative strength of the two colors, population and electron scattering effects for the two states are investigated at different operating temperatures and in the presence of a strong magnetic field. At elevated temperatures, the population of state $|3\rangle$ is continuously reduced, resulting in only the 3.8 THz transition lasing at 140 K. For an applied magnetic field, the elastic scattering channel from $|4\rangle \rightarrow |3\rangle$ is progressively suppressed, resulting in laser emission switching from 3.4 THz to 3.8 THz.

Quantum Cascade lasers (QCLs) in the terahertz frequency range have become significantly improved in recent years.[1] These improvements have enabled lasing up to 200 K,[2] a maximum output power of 1 W,[3] and octave spanning devices.[4] Accurate knowledge of electronic energy states in Quantum Cascade heterostructures is indispensable for the design of broadband laser structures and active regions with high maximum operating temperatures (T_{max}). Both features require a good understanding of how the individual quantized electron states contribute to the overall lasing performance. A broadband terahertz QCL gain medium is desired especially when it comes to enabling frequency combs[5] or ultrashort pulse generation.[6] The most efficient way to create broadband terahertz QCL active regions is to grow heterogeneous Quantum Cascade structures consisting of multiple subactive regions centered at different frequencies.[7] This technique allows us to add the gain bandwidth of each subactive region and has enabled octave-spanning emission for terahertz QCLs, lasing from 1.64 to 3.35 THz by stacking three different active regions.[4]

High operating temperatures for terahertz QCLs are an ongoing challenge since their first demonstration in 2002.[8] Up to now, the record operating temperature T_{max} is 200 K,[2] which was achieved by using a three-well active region design with a resonant LO-phonon depopulation mechanism.[9,10] To increase this temperature, different active region designs were studied, including two-well designs,[11,12] double-phonon depopulation designs,[13] and a higher barrier for reduced electron leakage.[14] Apart from alternative designs, novel material systems with a lower effective electron mass m_e^* were studied, because the optical gain is proportional to $(m_e^*)^{-3/2}$.[15] Such material systems include InGaAs/In(Ga)AlAs,[16–19] InGaAs/GaAsSb,[20] and InAs/AlAsSb[21] with material compositions lattice matched to InP and InAs. Up to now, neither alternative designs nor novel material system could surpass the operating temperature of 200 K.

A narrower spectral gain of the active region is a strategy to improve the temperature performance of existing designs. Calculations based on the nonequilibrium Green's functions method[22] or using a Monte Carlo approach[23] can be used to describe the gain profile of terahertz QCLs. Terahertz time-domain spectroscopy measurements provide valuable information like spectral gain profile[24] and gain dynamics[25,26] and can be used to improve the performance of active region designs. Another approach for understanding gain broadening processes is to study the dominant scattering mechanisms (impurity

and electron-electron scattering) between the different energy levels. One method to study these scattering mechanisms is to apply a magnetic field perpendicular to the plane of the layer structure.[27] The device performance of terahertz QCLs is modified dramatically in the presence of a magnetic field. The suppression of nonradiative relaxation channels reduces the threshold current density[28] and allows higher operating temperatures. For a GaAs/AlGaAs based terahertz QCL, T_{max} of 225 K at a magnetic field of 19.3 T was achieved.[29] The lower effective mass of InGaAs reduces the required magnetic field, resulting in 190 K at 11 T for InGaAs/GaAsSb[30] and 195 K at 12 T for InGaAs/InAlAs[31] terahertz QCLs.

In the present study, we investigate a dual-color GaAs/AlGaAs terahertz QCL with two upper laser states to study the influence of the operating temperature on the preferred lasing transition and compare it to band structure calculations. To obtain information on scattering mechanisms for the population of the two upper laser states, we apply a magnetic field parallel to the grow direction and find for higher B-fields a progressive switching of the emission intensity from one lasing colors to the other.

The used QCL design is a three-well active region with an aluminum concentration of 21% in the barrier to suppress electron leakage at elevated temperatures, resulting in $T_{max} = 196$ K at a frequency of 3.8 THz.[14] The active region is processed in metal-metal waveguide geometry to ensure high mode confinement and low optical losses. For multimode lasing, nickel side absorbers are added in the processing step to suppress higher order lateral modes.[6]

Figure 1(a) shows the lasing transitions of the investigated three-well design at bias fields of 12.2 and 12.5 kV cm^{-1}. The two upper laser states and lower laser state are marked as levels $|4\rangle$, $|3\rangle$, and $|2\rangle$. The two different lasing transitions are marked as LT$_{32}$ and LT$_{42}$ for the transitions $|3\rangle \rightarrow |2\rangle$ and $|4\rangle \rightarrow |2\rangle$, respectively. Level $|1\rangle$ is the extraction state, which is efficiently depopulated by a LO-phonon emission to the injector state of the next period. Compared to other three-well quantum cascade structures,[2,10] the injector barrier of this structure is more pronounced due to its higher Al concentration. This results in a small energy separation between the injector level $|4\rangle$ and the upper laser level $|3\rangle$ of $E_{43} = 1.75$ meV (compared to 2.3 meV and 2.9 meV in Refs. 10 and 2, respectively) and furthermore in a similar

oscillator strength for both transitions of these two energy states to the lower laser level $|2\rangle$ (f_{42} and f_{32}). To calculate the spectral gain profile of the structure for different bias fields, we use a simple model based on the calculation of the spectral gain cross-section[32]

$$g_i(\omega) = \frac{2\pi e^2 z_i^2}{\epsilon_0 n_{ref} L \lambda_i} \frac{\gamma}{(E_i - \hbar\omega)^2 + \gamma^2}, \quad (1)$$

where e is the electron charge, z_i is the dipole matrix element for the two states that contribute to the gain, $n_{ref} = 3.6$ is the refractive index, λ_i is the wavelength for each transition, $\gamma = 1$ meV is the assumed level broadening, and E_i is the energy of the relevant transitions. Figure 1(b) shows the combined gain cross-section of transition LT$_{32}$ and LT$_{42}$ for bias fields in the range from 12.1 to 12.5 kV cm^{-1}, where a linear offset in the y-axis is added for each bias point to enhance the clarity. For low bias fields, the main part of the gain is located at LT$_{42}$, which changes to transition LT$_{32}$ for higher bias fields. Beside this, a blueshift can be seen for both transitions induced by the Stark effect.

The spectrum in Fig. 1(c) shows multimode lasing and two separated lasing regions at 3.4 THz and 3.8 THz which correspond to an energy difference of $\Delta E = 1.65$ meV. This is in good agreement with the energy difference of the injector and upper laser state E_{43} obtained from band structure calculations done with a 1-dimensional Schrödinger solver. With this dual-color emission, our QCL structure is well suited to study the population of each of the two upper laser states as well as the interaction between them. This is very important for understanding the injection process and provides a possibility for controlled switching of terahertz colors. While the bias dependence of the matrix elements is quite clear, the emission intensity also depends on the population of each of the two levels.

To investigate the bias dependent emission color at different temperatures, the processed samples are mounted on the cold finger of a continuous flow cryostat. The emitted terahertz radiation is collected with a parabolic mirror and guided into a Fourier-transform infrared (FTIR) spectrometer with an integrated deuterated triglycine sulfate (DTGS) terahertz detector. Figure 2(a) shows the light–current–voltage (LIV) measurements at heat sink temperatures of 5 K, 80 K, and 140 K. For the LIV measurements, the device (2550 μm long and 120 μm wide, with a 15 μm nickel side absorber) is driven with a pulse length of 500 ns and a repetition rate of 10 kHz (0.5% duty cycle) to prevent heating of the structure during laser operation. The colored dots represent the operating points ranging from lasing threshold up to the maximum intensity for the measured spectra shown in Fig. 2(b). For all temperatures, the lasing spectra at threshold start with a frequency of 3.8 THz corresponding to the transition LT$_{42}$. This matches our calculation of the gain cross-section, which shows higher gain for this transition at lower bias fields [compare Fig. 1(c)]. For the two low temperature measurements, transition LT$_{32}$ appears for higher current densities and thus higher bias fields, whereas for the measurement at 140 K, this transition does not occur anymore. It also becomes apparent that the intensity of LT$_{32}$ is already reduced at 80 K. Although thermally activated energy distribution among the two states is expected at an elevated temperature, the wide injector barrier prevents a sufficient population of state $|3\rangle$ and reduces the lasing transition LT$_{32}$. This shows that the spectral gain cross-section, calculated with a 1-D Schrödinger solver, cannot explain the obtained spectral mode formation, since a more precise knowledge of the population density of each state is required.
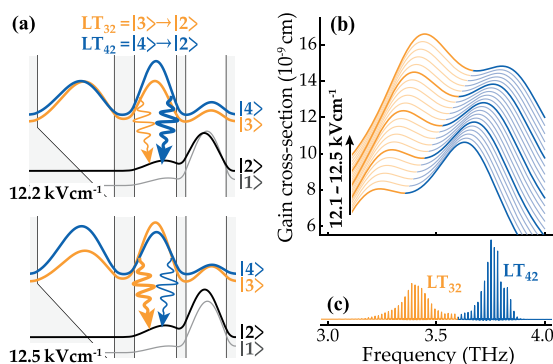
FIG. 1. (a) Band structure of the investigated design for two different bias fields. At 12.2 kV cm^{-1}, the transition LT$_{42}$ has a larger matrix element compared to LT$_{32}$. This changes for a bias field of 12.5 kV cm^{-1}. (b) Spectral gain cross-section for the two transitions calculated with Eq. (1) from 12.1 to 12.5 kV cm^{-1}. (c) Lasing spectrum at a temperature of 5 K showing two lasing bands belonging to the transitions LT$_{32}$ and LT$_{42}$.
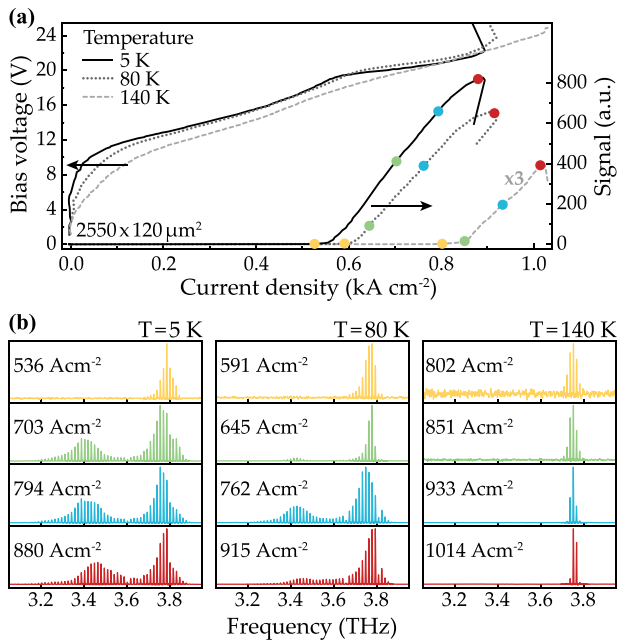
FIG. 2. (a) Light–current–voltage measurement for heat sink temperatures of 5 K, 80 K, and 140 K. The colored dots show the operation points for the measured spectra. (b) Spectra at different current densities for the three temperatures.

FIG. 3. (a) Magnetic field dependent LIV measurements at LHe temperature. (b) Schematic of the used setup. (c) Threshold current density and maximum signal against magnetic field B. (d) Spectra for different magnetic fields and bias voltages. Transition LT$_{32}$ is colored in orange and LT$_{42}$ in blue. (e) Integrated spectra for the two lasing transitions for different magnetic fields (B = 0 T, 3.75 T, and 7.5 T).

The low temperature spectra show a blueshift for transition LT$_{32}$ for increasing current densities. The center frequency increases from 3.4 THz to 3.46 THz. Compared to the gain cross-section calculation, the increase in 0.06 THz corresponds to a changed bias field of 0.1 kV cm^{-1}. Although the calculation of the gain cross-section also predicts a blueshift for LT$_{42}$, the spectra show that this transition is frequency stable. This behavior can be explained by the fact that state $|4\rangle$ is more localized at the doped injector well and the space charge there leads to a different voltage drop vs state $|3\rangle$. However, an alternative explanation could be that the two different lasing transitions are spatially separated in different Quantum Cascade periods due to the formation of electric field domains in the active region. To contradict the latter assumption and verify that both transitions LT$_{42}$ and LT$_{32}$ occur together in the same period inside the active region, we apply a magnetic field. Thereby, we investigate the scattering induced interaction of the two electron states of both upper laser levels.

The measurements are performed in a cryostat with a superconducting magnet providing a magnetic field up to 7.5 T. The laser device (1900 μm long and 90 μm wide, with a 10 μm nickel side absorber) is mounted on a probe, which is immersed in liquid helium (LHe) [see Fig. 3(b)]. This guarantees a stable operating temperature of 4.2 K. The magnetic field is applied parallel to the growth direction in order to achieve an in-plane confinement of the electrons. The individual intersubband energy states $|i\rangle$ split into a set of equidistant Landau levels $|i, n\rangle$ [with $E_{i,n} = E_i + (n + 1/2)\hbar\omega_c$], separated by the cyclotron energy $\hbar\omega_c = \hbar e B/m^*$, where e is the electron charge and $m^* = 0.067 m_0$ is the effective electron mass in GaAs. The emitted light is collected by a small parabolic mirror and guided via a light pipe to the FTIR spectrometer. For the LIV measurements [see Fig. 3(a)], the duty cycle is increased to 1% to compensate for the optical losses in the light pipe.

Figure 3(c) shows the threshold current density J$_{th}$ and the maximum lasing intensity as a function of the magnetic field B. For moderate B-fields up to 3 T, the emission intensity raises slightly and then starts to decrease. The threshold current density decreases for higher B-fields, which is a result of the reduced nonradiative scattering processes. For magnetic fields higher than 6 T, J$_{th}$ increases again, which can be explained by the reopening of the elastic scattering channel.

To distinguish between the two intensities of transitions LT$_{32}$ and LT$_{42}$, spectra were recorded for several different operation points. Figure 3(d) shows the spectra for magnetic fields of 0 T, 3.75 T, and 7.5 T, which belong to the operation points marked in the light–current curve of Fig. 3(a), where the transitions LT$_{32}$ and LT$_{42}$ are colored orange and blue, respectively. The integrated signal for each of these two transitions is shown in Fig. 3(e). For B = 0 T, the transition LT$_{32}$ is clearly dominant, while for B > 1 T, the quantizing magnetic field reduces the elastic scattering from $|4\rangle$ to $|3\rangle$ and changes the electron population density of these two states. This leads to a reduced emission for LT$_{32}$ and a more pronounced intensity for LT$_{42}$ at a magnetic field of 3.75 T. For the highest magnetic field (B = 7.5 T), transition LT$_{32}$ vanishes completely due to the crossing of the Landau levels $|3, 0\rangle$ and $|2, 1\rangle$.

A full scan of the frequency resolved QCL emission as a function of the magnetic field and applied bias voltage is shown in Fig. 4. In the lower panel, the Landau fan for the involved two upper laser states $|3, n\rangle$ and $|4, n\rangle$ as well as the lower laser state $|2, n\rangle$ is shown. Due to
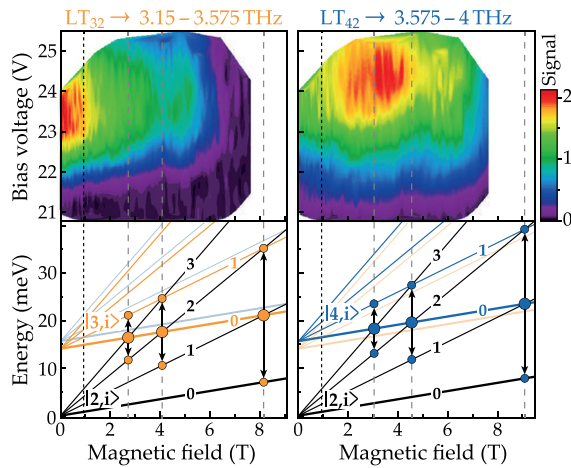
FIG. 4. QCL emission plotted as a function of the magnetic field and applied bias voltage for LT_{32} and LT_{42} in the left and right maps, respectively. The Landau fan chart of the involved states is depicted below. As an example of Auger scattering processes, the transition of two electrons from state $|3,0\rangle$ to the states $|3,1\rangle$ and $|2,0\rangle$ at 8.2 T is shown.

the low nonparabolicity of GaAs, we do not consider the nonparabolic correction. The crossings of $|2,n=1,2,3\rangle$ with $|3,0\rangle$ and $|4,0\rangle$ are marked with gray vertical dashed lines for the left and right maps.

Around 8.2 T, there is a crossing between the $|3,0\rangle$ and $|2,1\rangle$ Landau levels. This crossing reopens the channel for elastic scattering that had been closed by the Landau quantization and thereby leads to a suppressed lasing action. In addition to these nonradiative transitions assisted by static disorder (in our case, most probably, impurity scattering), there is an energy coincidence between the cyclotron resonance transition between the Landau levels attached to both the $|2\rangle$ and $|3\rangle$ states and the intersubband energy $E_3 - E_2$. Under such a circumstance, it has been shown[33,34] that, despite the small electron concentration in terahertz QCLs (here 3.5×10^{10} cm^{-2}), an efficient Auger scattering takes place at the magnetic field where two electrons in $|3,0\rangle$ are ejected by the electron–electron interaction, respectively, in $|3,1\rangle$ and $|2,0\rangle$ according to $E_3 - E_2 = \hbar\omega_c$. The same scenario repeats around 4.1 T and 2.7 T with Auger final states being $|3,1\rangle$ and $|2,1\rangle$ and $|3,1\rangle$ and $|2,2\rangle$, respectively. A plausible intrinsic reason why the Auger effect can be so efficient lays in the peaked aspect of the one and two electron densities of states of free electrons in a quantizing B-field. Within the Fermi Golden rule approach, the scattering frequency of an initial two electron $|3,0\rangle$ state behaves like the integral of the density of states of the first electron at $|3,1\rangle$ ($\rho(\epsilon_I - E_3 - 3/2\hbar\omega_c)$) times that of the second electron at $|2,0\rangle$ ($\rho(\epsilon_{II} - E_2 - 1/2\hbar\omega_c)$), restricted by the energy condition $\delta(\epsilon_I - \epsilon_{II} - 2\hbar\omega_c)$. This leads to a huge number of final states and therefore to a very short level lifetime, when the resonance condition $E_3 + 1/2\hbar\omega_c = E_2 + 3/2\hbar\omega_c$ is fulfilled. For the other Auger resonances located around 4.1 T and 2.7 T, the same argument would hold, except for the fact that the one electron densities of states are smaller at these smaller B-fields. This whole argument can also be applied to the crossing of Landau level $|4,0\rangle$ and $|2,1\rangle$ at around 9.1 T and explains the reduced laser emission of LT_{42} at 7.5 T.

At zero magnetic field, electrons injected in the subband of level $|4\rangle$ can be elastically scattered to the subband of $|3\rangle$. This is considered

to be a rather efficient process because the small energy difference between $|3\rangle$ and $|4\rangle$ implies a small wavevector exchange between the initial $|4\mathbf{k}\rangle$ and the final $|3\mathbf{k}'\rangle$ states, an advantage for Coulombic scattering. When the electrons enter the quantizing regime due to a strong enough B-field, these elastic scattering channels are progressively suppressed and what remains for populating the Landau levels attached to $|3\rangle$ from those attached to $|4\rangle$ is the acoustical phonon emission, very ineffective at low temperature or the Auger effect. The latter is hindered by two electron energy conservation at fields $B > m^*(E_4 - E_3)/(\hbar e) \approx 1$ T (marked as a vertical black dashed line in Fig. 4). Thus, the electron supply to the Landau levels attached to $|3\rangle$ by those injected in the Landau levels attached to $|4\rangle$ is progressively quenched with the increasing B–field and leads to a switching of the predominant emission color from LT_{32} to LT_{42}.

In conclusion, by studying a terahertz QCL with pronounced dual-color emission from two upper laser states, we have found that the operating temperature and an applied magnetic field have a strong influence on the lasing behavior of a dual-color terahertz QCL emitting at 3.4 THz and 3.8 THz. The dual transition lasing is achieved by using an active region with a low energy spacing of the injector and upper laser state and a similar matrix element of these two states with the lower laser level. Spectral measurements show lasing of transition LT_{42} at threshold for all investigated temperatures. At elevated temperatures, the population from state $|4\rangle$ to state $|3\rangle$ is reduced and decreases the population inversion for transition LT_{32} and hence also the lasing emission from this lasing band at 3.4 THz. This shows that—despite the small energy separation between the two upper states—the population between them is not thermalized. This is particularly important for the design of new high temperature active regions, enabling lasing above 200 K. Measurements with an applied magnetic field perpendicular to the layer structure show the mutual influence of the two lasing bands at low temperature. Strong magnetic fields suppress the elastic electron scattering from state $|4\rangle$ to $|3\rangle$ and enhance the lasing emission of LT_{43} at 3.8 THz. The results show that both upper states have an independent population which interact through inelastic scattering. With the magnetic field, the scattering channels can be controlled very precisely and thus the emission color can be switched.

REFERENCES

[1] B. S. Williams, Nat. Photonics **1**, 517 (2007).
[2] S. Fathololoumi, E. Dupont, C. Chan, Z. Wasilewski, S. Laframboise, D. Ban, A. Mátyás, C. Jirauschek, Q. Hu, and H. C. Liu, Opt. Express **20**, 3866 (2012).
[3] L. Li, L. Chen, J. Zhu, J. Freeman, P. Dean, A. Valavanis, A. Davies, and E. Linfield, Electron. Lett. **50**, 309 (2014).
[4] M. Rösch, G. Scalari, M. Beck, and J. Faist, Nat. Photonics **9**, 42 (2014).
[5] D. Burghoff, T.-Y. Kao, N. Han, C. W. I. Chan, X. Cai, Y. Yang, D. J. Hayton, J.-R. Gao, J. L. Reno, and Q. Hu, Nat. Photonics **8**, 462 (2014).
[6] D. Bachmann, M. Rösch, M. J. Süess, M. Beck, K. Unterrainer, J. Darmo, J. Faist, and G. Scalari, Optica **3**, 1087 (2016).

[7]D. Turčinková, G. Scalari, F. Castellano, M. I. Amanti, M. Beck, and J. Faist, Appl. Phys. Lett. **99**, 191104 (2011).

[8]R. Köhler, A. Tredicucci, F. Beltram, H. E. Beere, E. H. Linfield, A. G. Davies, D. A. Ritchie, R. C. Iotti, and F. Rossi, Nature **417**, 156 (2002).

[9]H. Luo, S. R. Laframboise, Z. R. Wasilewski, G. C. Aers, H. C. Liu, and J. C. Cao, Appl. Phys. Lett. **90**, 041112 (2007).

[10]S. Kumar, Q. Hu, and J. L. Reno, Appl. Phys. Lett. **94**, 131105 (2009).

[11]M. Franckié, L. Bosco, M. Beck, C. Bonzon, E. Mavrona, G. Scalari, A. Wacker, and J. Faist, Appl. Phys. Lett. **112**, 021104 (2018).

[12]S. Kumar, C. W. I. Chan, Q. Hu, and J. L. Reno, Appl. Phys. Lett. **95**, 141110 (2009).

[13]R. W. Adams, K. Vijayraghavan, Q. J. Wang, J. Fan, F. Capasso, S. P. Khanna, A. G. Davies, E. H. Linfield, and M. A. Belkin, Appl. Phys. Lett. **97**, 131111 (2010).

[14]M. A. Kainz, S. Schönhuber, A. M. Andrews, H. Detz, B. Limbacher, G. Strasser, and K. Unterrainer, ACS Photonics **5**, 4687 (2018).

[15]E. Benveniste, A. Vasanelli, A. Delteil, J. Devenson, R. Teissier, A. Baranov, A. M. Andrews, G. Strasser, I. Sagnes, and C. Sirtori, Appl. Phys. Lett. **93**, 131108 (2008).

[16]C. Deutsch, M. A. Kainz, M. Krall, M. Brandstetter, D. Bachmann, S. Schönhuber, H. Detz, T. Zederbauer, D. MacFarland, A. M. Andrews, W. Schrenk, M. Beck, K. Ohtani, J. Faist, G. Strasser, and K. Unterrainer, ACS Photonics **4**, 957 (2017).

[17]H. Detz, A. M. Andrews, M. A. Kainz, S. Schönhuber, T. Zederbauer, D. MacFarland, M. Krall, C. Deutsch, M. Brandstetter, P. Klang, W. Schrenk, K. Unterrainer, and G. Strasser, Phys. Status Solidi A **216**, 1800504 (2018).

[18]L. Ajili, G. Scalari, N. Hoyler, M. Giovannini, and J. Faist, Appl. Phys. Lett. **87**, 141107 (2005).

[19]K. Ohtani, M. Beck, G. Scalari, and J. Faist, Appl. Phys. Lett. **103**, 041103 (2013).

[20]C. Deutsch, A. Benz, H. Detz, P. Klang, M. Nobile, A. M. Andrews, W. Schrenk, T. Kubis, P. Vogl, G. Strasser, and K. Unterrainer, Appl. Phys. Lett. **97**, 261110 (2010).

[21]M. Brandstetter, M. A. Kainz, T. Zederbauer, M. Krall, S. Schönhuber, H. Detz, W. Schrenk, A. M. Andrews, G. Strasser, and K. Unterrainer, Appl. Phys. Lett. **108**, 011109 (2016).

[22]R. Nelander and A. Wacker, Appl. Phys. Lett. **92**, 081102 (2008).

[23]C. Jirauschek and P. Lugli, J. Appl. Phys. **105**, 123102 (2009).

[24]D. Bachmann, M. Rösch, C. Deutsch, M. Krall, G. Scalari, M. Beck, J. Faist, K. Unterrainer, and J. Darmo, Appl. Phys. Lett. **105**, 181118 (2014).

[25]C. G. Derntl, G. Scalari, D. Bachmann, M. Beck, J. Faist, K. Unterrainer, and J. Darmo, Appl. Phys. Lett. **113**, 181102 (2018).

[26]D. R. Bacon, J. R. Freeman, R. A. Mohandas, L. Li, E. H. Linfield, A. G. Davies, and P. Dean, Appl. Phys. Lett. **108**, 081104 (2016).

[27]A. Leuliet, A. Vasanelli, A. Wade, G. Fedorov, D. Smirnov, G. Bastard, and C. Sirtori, Phys. Rev. B **73**, 085311 (2006).

[28]G. Scalari, C. Walther, M. Fischer, R. Terazzi, H. Beere, D. Ritchie, and J. Faist, Laser Photonics Rev. **3**, 45 (2009).

[29]A. Wade, G. Fedorov, D. Smirnov, S. Kumar, B. S. Williams, Q. Hu, and J. L. Reno, Nat. Photonics **3**, 41 (2009).

[30]S. Maëro, L.-A. de Vaulchier, Y. Guldner, C. Deutsch, M. Krall, T. Zederbauer, G. Strasser, and K. Unterrainer, Appl. Phys. Lett. **103**, 051116 (2013).

[31]F. Valmorra, G. Scalari, K. Ohtani, M. Beck, and J. Faist, New J. Phys. **17**, 023050 (2015).

[32]J. Faist, *Quantum Cascade Lasers*, 1st ed. (Oxford University Press, Oxford, United Kingdom, 2013).

[33]F.-R. Jasnot, L.-A. de Vaulchier, Y. Guldner, G. Bastard, A. Vasanelli, C. Manquest, C. Sirtori, M. Beck, and J. Faist, Appl. Phys. Lett. **100**, 102103 (2012).

[34]G. Scalari, S. Blaser, J. Faist, H. Beere, E. Linfield, D. Ritchie, and G. Davies, Phys. Rev. Lett. **93**, 237403 (2004).